Damage Detection in Composite Aircraft Fuselages Under Load and Temperature Using Gaussian Processes for GW-SHM

MARIA MOIX-BONET, DANILE SCHMIDT,
BENJAMIN ECKSTEIN and PETER WIERACH

ABSTRACT

A full-scale composite door surrounding aircraft structure was instrumented with a GW-SHM system and subjected to three representative quasi-static load cases using a hydraulic test rig and broad temperature variations throughout the experiment. A data-driven approach based on Gaussian Processes is used to detect barely visible impact damage introduced during the test campaign, differentiating between benign environmental/operational conditions and barely visible impact damage.

INTRODUCTION

The design of aircraft structures has evolved over the decades, with the introduction of composite materials leading to new requirements for damage tolerance and structural integrity ([1]). The integration of composite materials in aeronautics offers numerous benefits, but also introduces unique challenges related to damage and failure modes.

Guided Wave-based Structural Health Monitoring (GW-SHM) has emerged as a promising technique for identifying defects in composite aircraft structures. This method employs a network of permanently installed sensors to generate and receive ultrasonic Guided Waves, allowing for the detection of subtle changes in the structure's integrity ([2], [3]). However, one of the primary challenges facing GW-SHM is the impact of environmental and operational conditions on its performance.

Aircraft structures are subject to a wide range of variation in operational and environmental conditions affecting Guided Waves propagation. This can compromise the effectiveness of GW-SHM systems, which often rely on limited baseline data to detect damage. Compensating for these changes remains an active area of research, with current techniques being challenged by the complex geometry and structural behavior of monitored structures and the simultaneous presence of multiple environmental and operational factors. Thus, this study focuses on using a GW-SHM system to monitor damage in a full-scale composite aircraft fuselage under varying load and temperature.

Moix-Bonet M., Schmidt D. and Wierach P., German Aerospace Center, Lilienthalplatz 7, 38108 Brunswick, Germany
Eckstein B., Airbus Operations GmbH, Airbus-Allee 1, 28199 Bremen, Germany

EXPERIMENTAL SETUP: An Aircraft Composite Panel

A composite fuselage structure was employed in this study, which is representative of a passenger door surrounding area found on wide-body aircraft, such as the Airbus A350. The test structure has dimensions of 4100 mm x 5700 mm and comprises multiple frames, stringers, windows, and a surrounding door structure ([4]).

A custom-designed Guided Wave-based Structural Health Monitoring (GW-SHM) system was integrated onto the fuselage panel. The GW-SHM system's key features include a robust transducer network, reliable transducer connections, and a modular architecture ([5]). This design ensures sensor reliability and practical applicability in an industrial setting.

The test rig described in [6] and illustrated in 1 was used to apply representative loads to the fuselage panel, simulating conditions encountered during flight. Three basic load cases were selected for this study: uniaxial tension, lateral bending left, and vertical bending down. 1 provides a visual representation of these selected load cases, including their orientation on a barrel level.

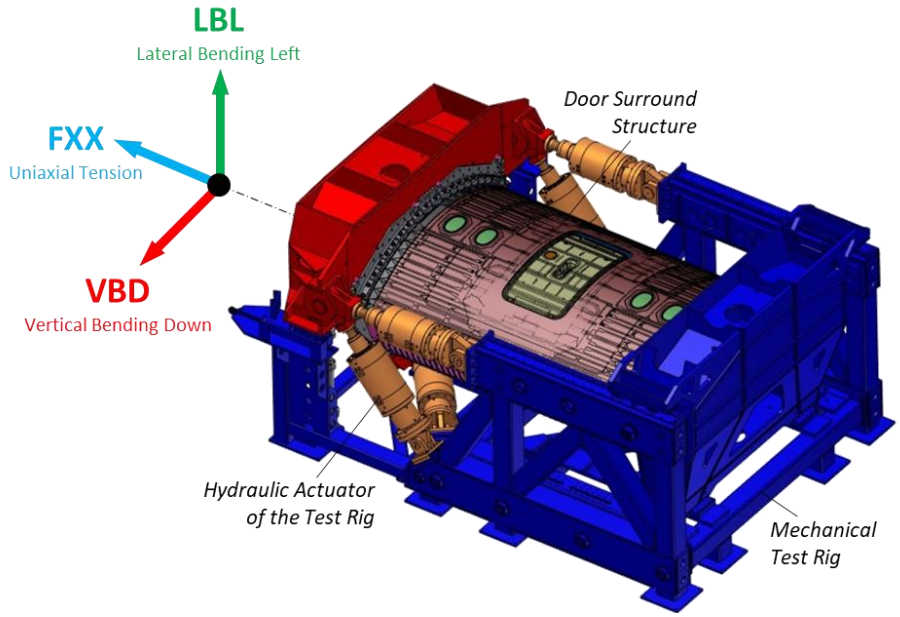

Figure 1. Composite Fuselage Panel in a Test Rig ([6])

To evaluate the suitability of the GW-SHM system, three load cases were applied in a quasi-static test until a load equivalent to 75% of the structure's Limit Load (LL) was reached. The quasi-static test was paused at multiple load steps between the unloaded condition and 75% LL to allow for measurements in static condition.

The test campaign was conducted in a non-climate-controlled hangar, resulting in GW-measurements being performed within a temperature range of 12°C to 30°C. This environment introduced additional variability in the data due to changes in temperature.

To introduce barely visible impact damage into the fuselage structure, impacts were applied using a gas gun, following the method described in [7]. Non-destructive inspection using phased array ultrasonics was performed at the impact locations to gather reference data.

METHODOLOGY: Gaussian Process Regression for Damage Detection

This section presents Gaussian Process Regression (GPR) as a method for detecting damage using a Guided Wave-Based Structural Health Monitoring (GW-SHM) system within the current application scenario: a composite fuselage structure subjected to multi-axial loading and temperature variations typical of a non-climatized hangar. A detailed description of the combined effects of load and temperature during this test campaign can be found in [8].

Gaussian Processes (GPs) have been increasingly applied in the field of SHM for various tasks, such as modeling time-series in vibration analysis [9], and quantifying damage using guided waves [10]. For a comprehensive guide on applying GPs to machine learning tasks, [11] provides an outstanding framework.

In this work, we employ GPR for unsupervised damage detection using GW-SHM. Specifically, GPR is used to connect a set of input operational variables with the resulting information from the GW-SHM system, utilizing temperature and load as input features and one or several selected signal features from the GW signals as the output variable.

In regression tasks, we often assume that the observed data y can be modeled as:

$$y = f(\mathbf{x}) + \epsilon \qquad \epsilon \sim \mathcal{N}(0, \sigma_n^2) \tag{1}$$

Where $\mathbf{x}$ is the input (feature vector), $f(\mathbf{x})$ is the unknown underlying function we aim to learn, and ϵ is the noise term, assumed to be Gaussian noise with zero mean and variance σ_n^2.

GPR approaches the regression problem by placing a prior over the function $f(\mathbf{x})$, assuming that for any finite set of inputs, the corresponding function values follow a joint Gaussian distribution:

$$f(\mathbf{x}) \sim \mathcal{GP}(m(\mathbf{x}), k(\mathbf{x}, \mathbf{x}')) \tag{2}$$

where $m(\mathbf{x})$ is the mean function and $k(\mathbf{x}, \mathbf{x}')$ is the covariance function.

The covariance function is defined by the choice of kernel, which specifies the set of possible functions the Gaussian process can represent. In this case, the squared exponential kernel is selected, known for producing smooth and infinitely differentiable functions. It is mathematically defined as:

$$k(x, x') = \exp\left(-\frac{\|x - x'\|^2}{2\ell^2}\right) \tag{3}$$

Where $\|x - x'\|$ is the Euclidean distance between inputs, and ℓ is the length-scale parameter controlling the smoothness.

Given a training dataset $\mathcal{D} = \{(\mathbf{X}, \mathbf{y})\}$, where $\mathbf{X} = [\boldsymbol{x_1}, \dots, \boldsymbol{x_n}]$ and $\mathbf{y} = [\boldsymbol{y_1}, \dots, \boldsymbol{y_n}]$, GPR computes the distribution over functions conditioned on the data. The process begins by calculating the covariance matrix K for all training points using the chosen kernel. Once the GPR model has been trained, classically in GPR, a new input $\mathbf{x}_*$ arrives and the predictive mean and variance at $\mathbf{x}_*$ is determined.

To achieve this, a joint covariance matrix is computed for the new input $\mathbf{x}_*$, representing the relationship between $\mathbf{x}_*$ and each training point. The joint distribution of the observed targets $\mathbf{y}$ and the function values at a new input $\mathbf{x}_*$ is:

$$\begin{bmatrix}\mathbf{y}\\ f_*\end{bmatrix} \sim \mathcal{N}\left(\mathbf{0}, \begin{bmatrix}K(\mathbf{X},\mathbf{X}) + \sigma_n^2 I & K(\mathbf{X},\mathbf{x}_*)\\ K(\mathbf{x}_*,\mathbf{X}) & k(\mathbf{x}_*,\mathbf{x}_*)\end{bmatrix}\right) \tag{4}$$

where $K(\mathbf{X},\mathbf{X})$ is the covariance matrix over training inputs, $K(\mathbf{X},\mathbf{x}_*)$ is the covariance vector between training inputs and the test point, and $k(\mathbf{x}_*,\mathbf{x}_*)$ is the covariance at the test point. Finally, the noise present in the training dataset is represented by σ_n^2.

The predictive distribution for the output f_* at the new input $\mathbf{x}_*$ is Gaussian with:

$$\bar{f}_* \triangleq \mathbb{E}[f_*] = K(\mathbf{x}_*,\mathbf{X})[K(\mathbf{X},\mathbf{X}) + \sigma_n^2 I]^{-1}\mathbf{y} \tag{5}$$

$$var[f_*] = K(\mathbf{x}_*,\mathbf{x}_*) - K(\mathbf{x}_*,\mathbf{X})[K(\mathbf{X},\mathbf{X}) + \sigma_n^2 I]^{-1}K(\mathbf{X},\mathbf{x}_*) \tag{6}$$

This provides both a mean prediction $\mathbb{E}[f_*]$ and an uncertainty estimate $var[f_*]$.

This represents the classical application of Gaussian Process Regression (GPR), where, after training, the model is employed to predict outcomes for new input data x_*. In the context of the current study, GPR is instead used for anomaly detection. Once the model has been trained, incoming data points are evaluated by calculating their likelihood under the GPR model. This likelihood assessment enables the identification of anomalies by determining whether new observations conform to the learned data distribution. The likelihood of observing the output y_* at input x_*, given the trained GPR model, is:

$$p(y_*|x_*,X,y) = \frac{1}{\sqrt{2\pi(var_{f_*} + \sigma_n^2)}}\exp\left(-\frac{(y_* - \bar{f}_*)^2}{2(var_{f_*} + \sigma_n^2)}\right) \tag{7}$$

If the likelihood $p(y_*|x_*,X,y)$ is very low, it suggests that y_* is unlikely under the current model, indicating a potential anomaly. Conversely, a high likelihood indicates the point fits well within the learned distribution.

RESULTS: Damage Detection for an Actuator-Sensor Path

This section demonstrates the damage detection method developed in this work by using one selected actuator-sensor path as example. The GP-based method previously described is applied to this path, which has been intentionally chosen to highlight the advantages of this approach. The combination of effects due to temperature, load, and damage in this path is complex, making it challenging to separate these influences without a well-suited model.

Figure 2 shows the filtered signal response between actuator 3 and sensor 7 at 70 kHz. All signals acquired for this path and frequency during the test campaign are plotted, including three load cases ranging from the unloaded condition to 75% of the limit load, as well as a temperature range from 12°C to 32°C. The first arrival of the signal is zoomed in to visualize the subtle differences in amplitude and time-of-flight.

In Figure 2(a), the pristine signal is plotted, with colors indicating the load level. A range of amplitudes and time-of-flights can be observed due to the varying load cases, load levels, and temperatures. Note that the strains in this region are relatively low compared to other areas of the structure, resulting in moderate changes in signal response due to changing load conditions. For comparison, results from highly loaded areas can be found in [8]

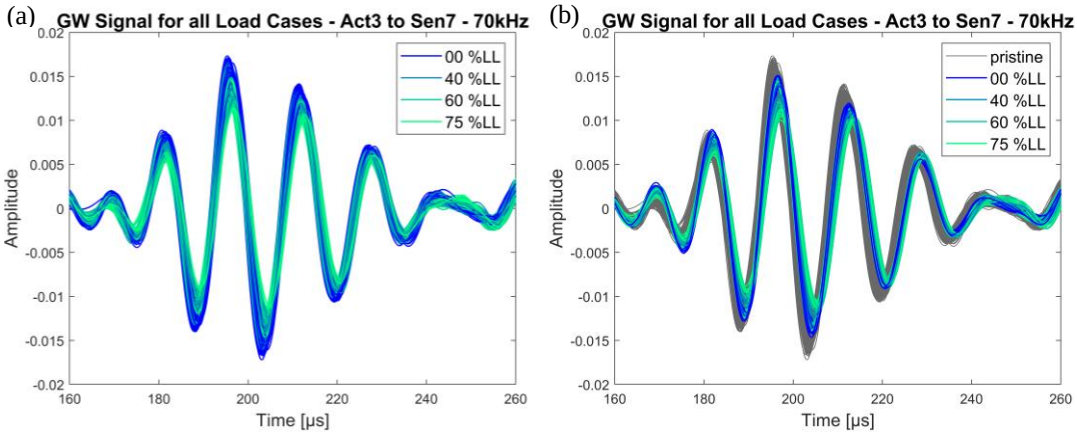

Figure 2: GW- Signal for Actuator 3 to Sensor 7 Path at 70kHz (a) in pristine state and (b) for pristine (grey) vs. damaged (color) state

The pristine signal response from Figure 2(a) is replotted in grey in Figure 2(b), with the damaged signal response superimposed on top, color-coded according to the load level. The shift due to damage is subtle, and the range of signal variations caused by changing load and temperature conditions makes it difficult to clearly differentiate between the pristine and damaged states in the raw signals. Although a general shift in amplitude and time-of-flight can be observed after damage occurrence, the change is not significant enough to reliably separate the pristine from the damaged state.

From the raw signals in Figure 2, two features are extracted: amplitude and time-of-flight (ToF). Figure 3 illustrates these two features for the path from actuator 3 to sensor 7, using three different color codes: load, temperature, and damage.

In Figure 3(a), the points representing the extracted features are color-coded according to the load level for the uniaxial tension load case. As the load level increases, the area covered by this actuator-sensor path undergoes compression. This results in a noticeable decrease in amplitude, while the ToF decreases minimally.

In Figure 3(b), the same features are colored according to the temperature at which they were acquired. Here, the dominant change in the features is an increase in amplitude with increasing temperatures, accompanied by a slight decrease in ToF.

The dataset consists of approximately 80% pristine condition data and 20% damaged state data. In Figure 3(c), the data is differentiated by the damage state of the structure. The signal from the damaged state generally exhibits a higher ToF; however, it is not clearly separable from the pristine state when considering all signal variations due to load and temperature.

Finally, Figure 3(d) presents an ultrasound C-Scan of the monitored damage, which consists of a delamination with a total size of 29-by-20 mm. The selected actuator-sensor path does not propagate directly through the center of the delamination but rather adjacent to it. As a result, the observed changes in the signal due to damage are minimal.

This specific case of small damage effect was intentionally chosen to demonstrate the advantages of the GP-based damage detection method.

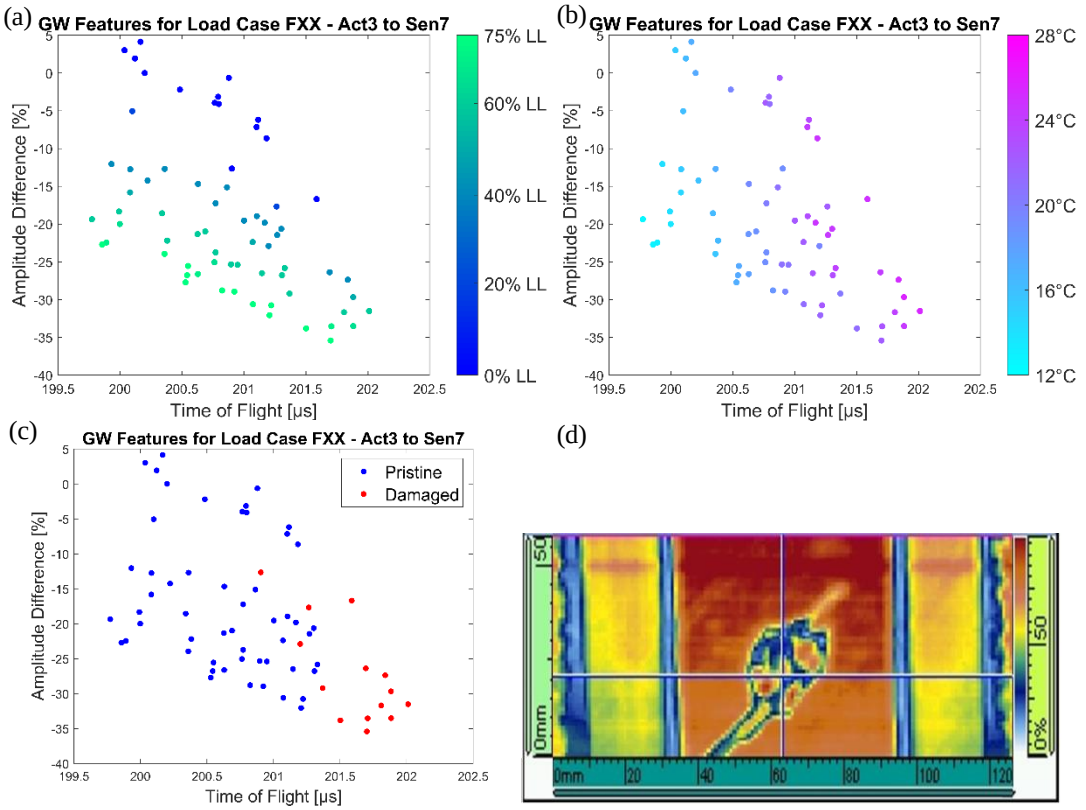

Figure 3: Amplitude and time-of-flight from GW-Signal for Actuator 3 to Sensor 7 Path at 70kHz plotted according to (a) temperature, (b) load, and (c) damage state

The next step involves performing GPR on the GW-signals acquired from the structure in its pristine state under varying conditions. For this purpose, load level and temperature are selected as independent variables, while time-of-flight (ToF) is used as the dependent variable. The limitation to three dimensions enables graphical representation of the GPR model, facilitating intuition-building around it.

Figure 4(a) presents a GPR model fitted to GW data acquired in a pristine state. The plot displays the observed time shift values over the two independent variables (load level and temperature) fitted in a GPR model, along with the 95% confidence bounds. The GPR fit reveals a monotonic increase in time shift for both higher temperatures and higher load levels.

Figure 4(b) provides a 2D cut of the 3D GPR fit, representing the model at a constant load level of 0% LL (unloaded state). The plot differentiates between points used for training, which are colored black for those at 0% load and grey for other load conditions. The colored points display the observed time shift values acquired during the unsupervised detection phase, where the color scale corresponds to the calculated likelihood or how well the fitted GPR model explains the new data.

The two marked data points, acquired after the impact event, clearly deviate from the 95% confidence bounds. One data point falls outside the temperature range available to train the GPR model. Therefore, the GPR presents a high variance in that temperature range. As a result, it is challenging for the model to identify the damage. In contrast, the

second point lies within the temperature and load ranges used for training, and its deviation from the fitted GPR model indicates an anomalous observation, suggesting potential damage.

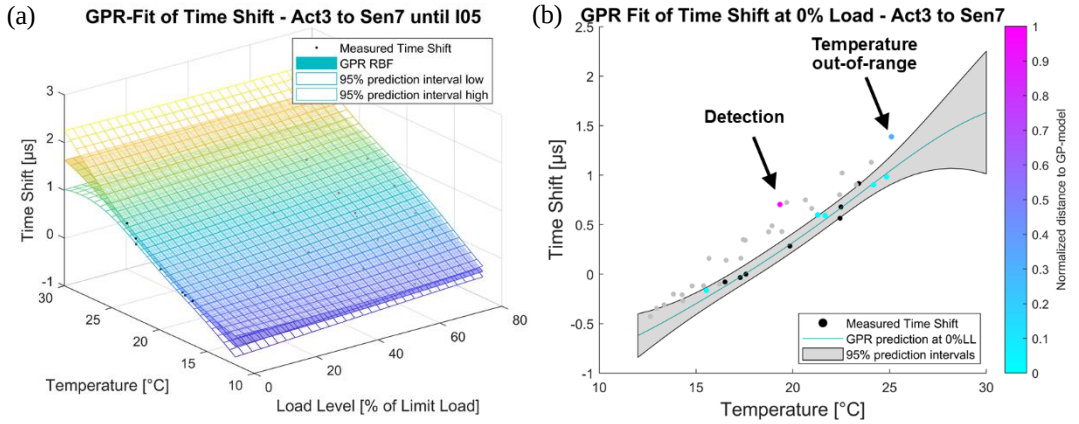

Fig. 4: (a) Gaussian Process Regression fitted on Time Shift for Actuator 3 to Sensor 7 Path
(b) GPR fit at 0% Load with Training and Test Data Points

The results show that excluding load information would not allow differentiation between operational conditions and damage, highlighting the importance of considering load effects in the architecture and signal processing design of GW-SHM-systems. The similarity in time shift between the anomalous points and those observed at other load levels (grey points) emphasizes the need to account for load effects when designing models for damage detection.

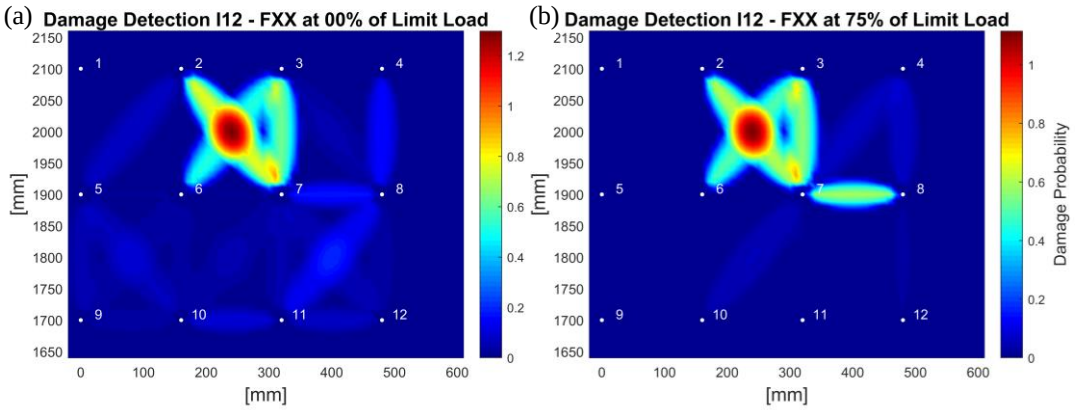

Figure 5: Likelihood-based Damage Detection with RAPID at (a) unloaded and (b) at 75% LL

In the final step, a damage index based on the likelihood is used in conjunction with a probability reconstruction algorithm, as formulated in [3]. For this purpose, the previously described procedure is applied to all actuator-sensor path in the given area. Figure 5 illustrates the damage detection performed for the impacted region, showing clear detection in two different load states: (a) the unloaded condition and (b) at 75% of the limit load for the uniaxial tension load case.

SUMMARY

A GW-SHM system has been installed on a representative composite fuselage structure. A full-scale test, including multi-axial mechanical loading and the introduction of barely visible impact damage, has generated a comprehensive dataset for the application of GW-SHM in realistic scenarios.

This study demonstrates the suitability of a GPR based approach for damage detection in a realistic scenario for aerospace structures. The results show that the GPR model can accurately differentiate between representative environmental and operational conditions and barely visible impact damage. The importance of considering load effects while building a data driven model for damage detection using GW-SHM is highlighted.

Future work will focus on generalizing the GPR approach to multi-axial loading conditions, as well as creating a GPR with multi-dimensional output to introduce more GW signal features in the model for a more robust damage detection.

ACKNOWLEDGEMENTS

We would like to express our gratitude for the support provided by the Federal Ministry of Economics and Climate Protection (BMWK) through their funding of this project under the LuFo VI framework concept, with grant agreement number 20D2105G.

REFERENCES

1. European Union Aviation Safety Agency. (2018). Easy Access Rules for Large Aeroplanes (CS-25)
2. Ricci, F., Monaco, E., Maio, L., Boffa, N. D., & Mal, A. K. (2016). Guided waves in a stiffened composite laminate with a delamination. Structural Health Monitoring, 15(3), 351–358.
3. Moix-Bonet, M., Eckstein, B., Loendersloot, R., & Wierach, P. (2015). Identification of Barely Visible Impact Damages on a Stiffened Composite Panel with a Probability-based Approach. 10th International Workshop on SHM.
4. Kruse, F., Kühn, M., Krombholz, C., Ucan, H., & Torstrick, S. (2015, September 2). Production of a Full Scale Demonstrator-Structure within the FP7 Project "Maaximus." 5th International Workshops on Aerostructures.
5. Schmidt, D., Moix-Bonet, M., Galiana, S., & Wierach, P. (2023, September). Integration von angepassten und dezentralen Structural Health Monitoring Systemen in Faserverbundstrukturen. Deutscher Luft- Und Raumfahrtkongress (DLRK).
6. Sachse, M., Götze, M., Nebel, S., Berssin, S., & Göpel, C. (2020). Testing approach for over wing doors using curved fuselage panel testing technology. Lecture Notes in Mechanical Engineering, 831–837.
7. Federal Aviation Administration. (2018). Certification and Compliance Considerations for Aircraft Products with Composite Materials.
8. Moix-Bonet, M., Schmidt, D., Eckstein, B., & Wierach, P. (2024). A Composite Fuselage under Mechanical Load: a case study for Guided Wave-based SHM. 11th European Workshop on SHM.
9. Avendaño-Valencia, L. D., Chatzi, E. N., & Tcherniak, D. (2020). Gaussian process models for mitigation of operational variability in the structural health monitoring of wind turbines. Mechanical Systems and Signal Processing, 142, 106686.
10. Amer, A., & Kopsaftopoulos, F. (2023). Gaussian process regression for active sensing probabilistic structural health monitoring: experimental assessment across multiple damage and loading scenarios. Structural Health Monitoring, 22(2), 1105-1139.
11. Rasmussen C.E., Williams C.B. (2006) Gaussian processes for machine learning. MIT Press.